Title

Subcellular activation of β-adrenergic receptors using a spatially restricted antagonist.

Journal

Proceedings of the National Academy of Sciences of the United States of America, 121(40)

Authors

Liccardo, Federica
Morstein, Johannes
Lin, Ting Yu
et al.

Publication Date

2024-10-01

DOI

10.1073/pnas.2404243121

Peer reviewed

PNAS RESEARCH ARTICLE | CELL BIOLOGY

Subcellular activation of β-adrenergic receptors using a spatially restricted antagonist

Federica Liccardo[a,b,1], Johannes Morstein[c,1], Ting-Yu Lin[a], Julius Pampel[c], Di Lang[a], Kevan M. Shokat[c,d], and Roshanak Irannejad[a,b,2]

Affiliations are included on p. 9.

Edited by Brian Kobilka, Stanford University School of Medicine, Stanford, CA; received February 28, 2024; accepted August 19, 2024

Gprotein-coupled receptors (GPCRs) regulate several physiological and pathological processes and represent the target of approximately 30% of Food and Drug Administration-approved drugs. GPCR-mediated signaling was thought to occur exclusively at the plasma membrane. However, recent studies have unveiled their presence and function at subcellular membrane compartments. There is a growing interest in studying compartmentalized signaling of GPCRs. This requires development of tools to separate GPCR signaling at the plasma membrane from the ones initiated at intracellular compartments. We leveraged the structural and pharmacological information available for β-adrenergic receptors (βARs) and focused on β1AR as exemplary GPCR that functions at subcellular compartments, and rationally designed spatially restricted antagonists. We generated a cell-impermeable βAR antagonist by conjugating a suitable pharmacophore to a sulfonate-containing fluorophore. This cell-impermeable antagonist only inhibited β1AR on the plasma membrane. In contrast, a cell-permeable βAR antagonist containing a nonsulfonated fluorophore efficiently inhibited both the plasma membrane and Golgi pools of β1ARs. Furthermore, the cell-impermeable antagonist selectively inhibited the phosphorylation of PKA downstream effectors near the plasma membrane, which regulate sarcoplasmic reticulum (SR) Ca^{2+} release in adult cardiomyocytes, while the β1AR Golgi pool remained active. Our tools offer promising avenues for investigating compartmentalized βAR signaling in various contexts, potentially advancing our understanding of βAR-mediated cellular responses in health and disease. They also offer a general strategy to study compartmentalized signaling for other GPCRs in various biological systems.

GPCR signaling | Pharmacology | drug design

Significance

Gprotein-coupled receptors (GPCRs) transmit signals from various subcellular compartments, including the plasma membrane, endosome, and the Golgi. Signaling from each of these cellular compartments regulates distinct cellular outcomes. Targeting GPCR signaling in a compartment-specific manner poses a challenge due to the limited spatial selectivity of most ligands. To overcome this limitation, we have developed a spatially restricted antagonist for the β-adrenergic receptors (βARs). This antagonist blocks β1AR signaling at the plasma membrane while leaving β1AR signaling at the Golgi active. Our approach not only facilitates the study of subcellular βARs signaling in health and disease but also offers a straightforward method to manipulate compartmentalized signaling of other GPCRs.

Gprotein-coupled receptors (GPCRs) are seven-transmembrane receptors that initiate Gprotein-mediated signal transduction upon ligand binding (1). Studies over the past decade have challenged the textbook model of GPCR signaling by revealing that GPCR signaling is not restricted to the plasma membrane but also occurs from subcellular compartments, such as the endosomes, the Golgi apparatus, and the nuclear membranes (2–12). The distinct role of subcellularly activated GPCR/Gprotein complexes remains to be fully understood. There are only a handful of studies demonstrating the cellular and physiological significance of GPCR signaling from subcellular locations (12). This limitation is partly due to lack of tools that would allow separating receptors' function at each location. Traditional tools for studying endosomal signaling are based on genetic or pharmacological manipulations of machineries such as clathrin and dynamin that regulate receptor trafficking to endosomes (2, 7, 8, 13–15). These types of manipulations disrupt trafficking of many other receptors and channels; thus, they can provoke unintended consequences or trigger compensatory mechanisms (16–18). Endosomal delivery of GPCR ligands, using pH-sensitive nanoparticle-encapsulated ligands, was further developed to better determine the consequence of GPCR activation at the endosomes (16, 19, 20). Further studies are necessary to improve the therapeutic efficacy of nanoparticle-encapsulated ligands (16). They are also limited to studying endosomal signaling and cannot be applied to functions of GPCRs that are located at the perinuclear/Golgi membranes.

To better pinpoint the consequence of compartmentalized GPCR signaling, our lab has previously taken advantage of nanobodies that were originally utilized for structural studies of monoamine GPCRs such as beta-adrenergic receptors (βARs) (21, 22). This is because these specific nanobodies bind to activated monoamine receptors (i.e., βARs) with high affinity and to the same region as Gproteins (6, 21, 22). Thus, when targeted to specific compartment, they can disrupt receptor coupling to the endogenous Gprotein through steric occlusion (6, 9, 11). Combining these tools with an inducible rapamycin dimerization system, we were able to test the significance of β1AR and D1DR signaling

Competing interest statement: K.M.S. has consulting agreements for the following companies, which involve monetary and/or stock compensation: Revolution Medicines, Black Diamond Therapeutics, BridGene Biosciences, Denali Therapeutics, Dice Molecules, eFFECTOR Therapeutics, Erasca, Genentech/Roche, Janssen Pharmaceuticals, Kumquat Biosciences, Kura Oncology, Mitokinin, Nested, Type6 Therapeutics, Venthera, Wellspring Biosciences (Araxes Pharma), Turning Point, Ikena, Initial Therapeutics, Vevo and BioTheryX.

This article is a PNAS Direct Submission.

[1]F.L. and J.M. contributed equally to this work.

[2]To whom correspondence may be addressed. Email: roshanak.irannejad@ucsf.edu.

This article contains supporting information online at https://www.pnas.org/lookup/suppl/doi:10.1073/pnas.2404243121/-/DCSupplemental.

Published September 27, 2024.

from the plasma membrane and the Golgi (9, 11, 23). While this strategy allows precise manipulation of compartmentalized signaling, it has certain shortcomings including lack of selective nanobodies for most GPCRs as well as insufficient delivery for in vivo studies. More recently, a similar approach has been developed based on the RGS domain of GRK2 to disrupt GPCR-Gq protein-mediated signaling at various subcellular compartments (24). While these strategies are useful for cell-based studies, they lack specificity for in vivo studies.

Given the growing interest in elucidating the physiological consequences of subcellular GPCRs' activity, there is an unmet need for developing pharmacological agonists and antagonists that could help resolve their spatial function in vitro and in vivo (25). Although several studies have already used available GPCR ligands that are relatively hydrophilic and thus predicted to be poorly membrane permeable (6, 9, 11, 23, 26–29), a number of reports suggest that some of these hydrophilic drugs can be transported across the lipid membrane by cationic or anionic membrane transporters (30–32). Therefore, the tissue expression pattern of membrane transporters could impact the consequences of subcellular GPCR activities.

In this study, we report the generation of a spatially restricted GPCR antagonist by focusing on β1AR, an exemplary GPCR. We modeled the common structural and chemical features of known βAR antagonists and coupled the pharmacophore of known antagonists to a sulfonated or nonsulfonated fluorophore, via click chemistry, to generate cell-impermeable and -permeable versions of the antagonists, respectively. Using a nanobody-based biosensor that allows for the detection of βAR activity in intact cells (6, 9), we first confirmed the selectivity of these antagonists at inhibiting distinct pools of β1ARs in cardiomyocytes. We then showed that the cell-impermeable β1AR antagonist specifically inhibits downstream effectors of PKA that are in the vicinity of the plasma membrane, without affecting PKA effectors that are known to be regulated by Golgi-localized β1AR signaling (33). This contrasts with a cell-permeable antagonist that inhibits both receptor pools. These drugs can be potentially employed in several biological systems and could allow the interrogation of compartmentalized βAR signaling both in vitro and in vivo.

Results

Organic Anion Transporter 1A2 (OATP1A2) Facilitates Transmembrane Transport of Sotalol in Murine Cardiomyocytes. We have previously shown that β1AR can become activated and couple to Gs protein at both the plasma membrane and the Golgi apparatus in cardiomyocytes (23, 33). To test whether pharmacological manipulation of β1AR signaling can be utilized to resolve their compartmentalized function, we tested already existing βAR antagonists possessing a range of hydrophobicity. Metoprolol, a hydrophobic/cell-permeable β1AR antagonist, can inhibit both the plasma membrane and Golgi pools of β1ARs in HeLa cells (9). In contrast, sotalol, a relatively hydrophilic and nonselective βAR antagonist (34) only inhibits the plasma membrane pool of β1AR in HeLa cells (9). Following up on this logic, we then tested sotalol to isolate the role of Golgi-β1AR signaling in cardiomyocytes derived from wild-type mice. We used our previously developed conformational sensitive nanobody-based biosensor, Nb80-GFP, to assess βARs activity in living cells (6, 9). We infected primary neonatal cardiomyocytes (NCM) with lentiviral constructs expressing β1AR and Nb80-GFP. In unstimulated β1AR expressing NCMs, Nb80-GFP expresses diffusely in the cytoplasm (Fig. 1 *A*, *Top* row). Upon treatment of NCMs with 10 μM dobutamine, a cell-permeable β1AR agonist, Nb80-GFP was recruited to activated β1AR at both the plasma membrane and the Golgi (Fig. 1 *A*, *Middle* and *Bottom* row, and Movie S1).

Having validated the response of Nb80-GFP in NCMs, we then tested the capability of sotalol in blocking the plasma membrane pool of β1AR. NCM expressing β1AR and Nb80-GFP were treated with 10 μM dobutamine and as expected we observed recruitment of Nb80-GFP in both PM and Golgi compartments (Fig. 1 *B*, *Upper* and *Middle* panel, and Movie S2). To our surprise, however, addition of 100 μM sotalol resulted in inhibition of both pools of β1AR, as indicated by loss of Nb80-GFP localization at the plasma membrane and the Golgi (Fig. 1 *B*, *Lower*). These results suggested that sotalol can reach the Golgi membrane and inhibit Golgi-localized β1AR in cardiomyocytes derived from wild-type mice.

To further confirm this result, we next assessed the effect of sotalol in inhibiting downstream effectors of β1AR signaling. Epinephrine stimulation of β1AR promotes phosphorylation of Ryanodine 2 receptors (RyR2), cardiac Troponin I (TnI), and Phospholamban (PLB) through PKA activation (35). We have previously established that PLB phosphorylation is mediated by activation of the Golgi-β1AR signaling (33). Thus, to test the effect of sotalol in blocking Golgi-β1AR signaling, we assessed PLB phosphorylation in isolated adult cardiomyocytes (ACM) derived from C57BL/6 mice. We first compared the efficacy of metoprolol and sotalol (*SI Appendix*, Fig. S1*A* and Dataset S1). Given that metoprolol is a more potent β1AR antagonist (*SI Appendix*, Fig. S1 *A* and *B*), we pretreated ACMs with various concentrations of sotalol (1, 10, and 100 μM) and compared the results to those of 10 μM metoprolol. We then stimulated ACMs with epinephrine, the endogenous full agonist of β1AR. Western blot analysis revealed that 10 and 100 μM sotalol treatment significantly block PLB phosphorylation and to the same extend as 10 μM metoprolol (Fig. 1*C**SI Appendix*, Fig. S1*C*). Altogether, these data suggest that sotalol can enter cardiomyocytes to inhibit Golgi-localized β1AR-mediated PLB phosphorylation (Fig. 1 *C* and *D* and *SI Appendix*, Fig. S1*C*, and Dataset S2).

One prediction would be that cardiomyocytes derived from mice express transporters that can facilitate sotalol transport. It has been reported that solute carrier OATP1A2 can transport anionic drugs such as sotalol across lipid bilayer (30, 31). We thus tested the expression of OATP1A2 and found that it is expressed in ACM derived from C57BL/6 mice (*SI Appendix*, Fig. S2 *A*–*C*). Importantly, endogenous OATP1A2 expressed at both the plasma membrane and the Golgi (*SI Appendix*, Fig. S2*A*). OATP1A2 staining was diminished when ACM were immunostained in the presence of OATP1A2 antibody blocking peptide (*SI Appendix*, Fig. S2*B*). OATP1A2 expression was also detected in NCMs derived from CD1 mice (*SI Appendix*, Fig. S1*C*). To test whether sotalol can be transported by OATP1A2, we then treated ACMs with naringin, a selective inhibitor of OATP1A2 (36, 37). Importantly, treatment of ACMs with 100 μM naringin blocked the effect of 10 μM sotalol on PLB phosphorylation. However, inhibition of RyR2 phosphorylation was unaffected by this treatment (Fig. 1 *E* and *F*, and Dataset S3). Altogether, these data suggest that OATP1A2 is expressed in ACMs derived from mice and can facilitate the transport sotalol into the cells to block Golgi-localized β1AR signaling.

Design and Synthesis of Cell-Permeable and -Impermeable βAR Antagonists. To overcome the limitation of facilitated transport of anionic drugs such as sotalol by OATP1A2, we sought to design impermeable antagonists of βARs, that cannot be transported into cells and can thus be used in multiple cell lines and model systems.

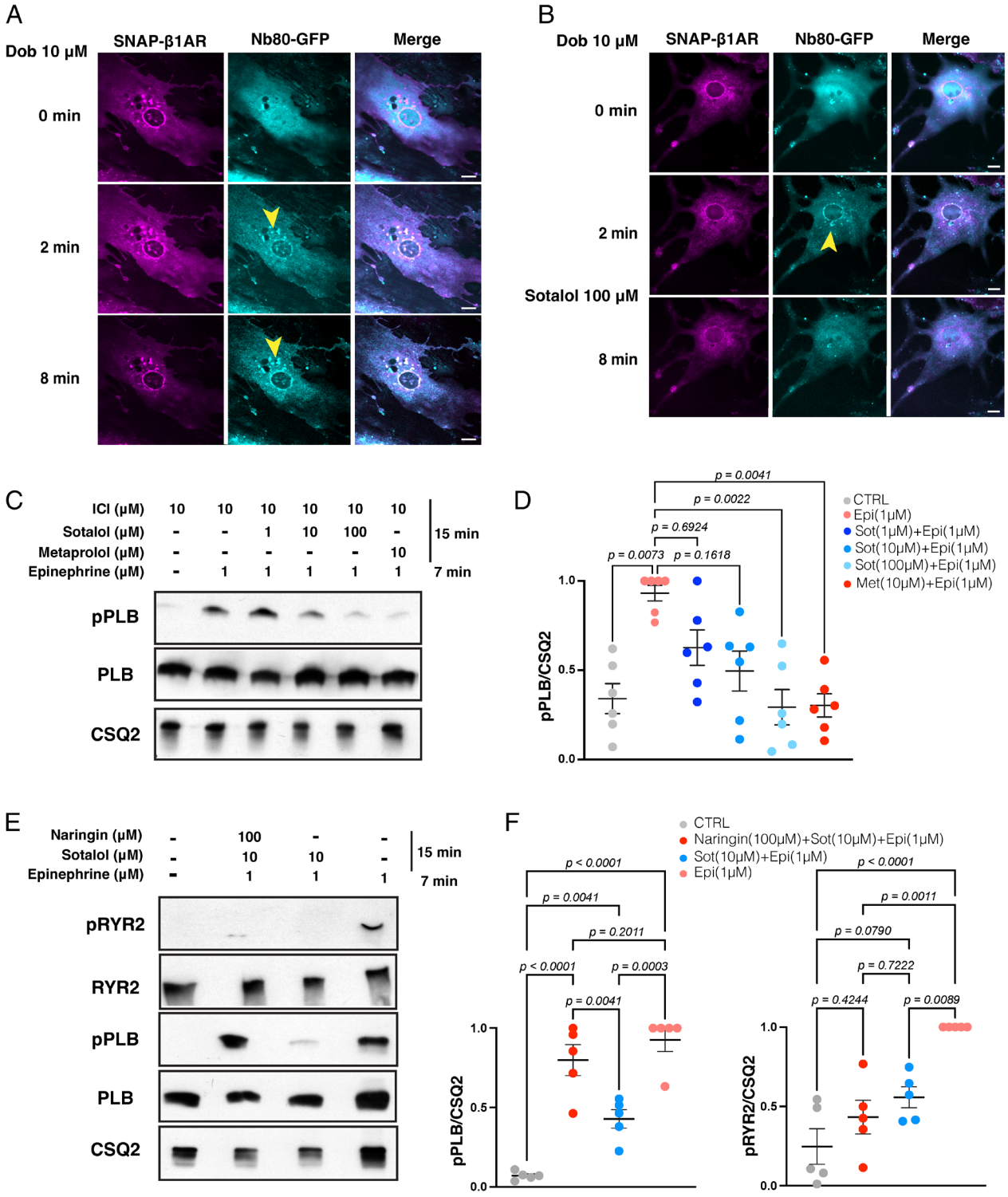

Fig. 1. Sotalol inhibits both the plasma membrane and the Golgi-localized β1AR in cardiomyocytes. (*A*) Representative confocal images of NCMs expressing the conformational biosensor of β1AR, Nb80-GFP (cyan), and SNAP-β1AR (magenta) before and after dobutamine (10 μM) treatment for 10 min. Stimulation with dobutamine (10 μM) results in Nb80-GFP recruitment to the plasma membrane and the Golgi. Arrowheads indicate Nb80-GFP localization at the Golgi. (Scale bar: 10 μm.) (*B*) Representative confocal images of NCMs expressing Nb80-GFP (cyan) and SNAP-β1AR (magenta) pretreated with dobutamine (10 μM) and before and after sotalol (100 μM) addition. Sotalol (100 μM) treatment for 3 min results in the loss of Nb80-GFP localization at the Golgi. Arrowheads indicate Nb80-GFP localization at the Golgi. (Scale bar: 10 μm.) (*C*) Representative phosphorylation profile of PLB (pPLB) regulated by β1AR in adult cardiomyocytes (ACM) derived from wild-type mice. ACM were pretreated with 10 μM β2AR-selective antagonist ICI-118551 (ICI) to isolate the function of β1AR. Phosphorylation of PLB Ser16/Thr17 (pPLB) was analyzed in wild-type ACM upon treatment with metoprolol (10 μM) or sotalol (1, 10, and 100 μM) for 15 min and followed by epinephrine (1 μM) treatment for 7 min at 37 °C. (*D*) Quantification of immunoblots of pPLB was normalized to the protein levels of CSQ2 and then reported as a percentage of the highest value in the groups. The quantified data from different experiments are presented as mean ± SEM. The *P*-values were calculated by two-way ANOVA. n = 6 independent biological replicates. (*E*) Representative phosphorylation profile of RyR2 (pRyR2) and PLB (pPLB) in ACM derived from wild-type mice. Phosphorylation of RyR2 Ser2808 (pRyR2) and PLB Ser16/Thr17 (pPLB) were analyzed upon treatment with OATP1A2-selective inhibitor Naringin (100 μM) for 15 min, sotalol (10 μM) for 15 min followed by epinephrine (1 μM) treatment for 7 min at 37 °C. (*F*) Quantification of immunoblots of pRyR2 and pPLB was normalized to the protein levels of CSQ2 and then reported as a percentage of the highest value in the groups. The quantified data from different experiments are presented as mean ± SEM. The *P*-values were calculated by two-way ANOVA. n = 5 independent biological replicates.

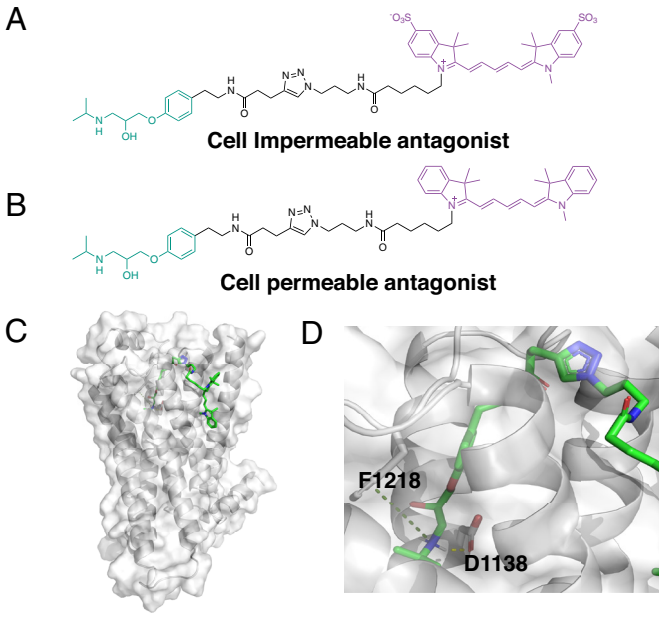

Fig. 2. Rational design and synthesis of spatially restricted βAR antagonists. (*A*) Chemical structures of cell-impermeable antagonist. Pharmacophore moiety of the antagonist (green) is functionalized with a linker (black) and a fluorophore (purple). The cell-impermeable antagonist is conjugated with a sulfonated Cy5. (*B*) Chemical structures of cell-permeable antagonist. Pharmacophore moiety of the antagonist (green) is functionalized with a linker (black) and a fluorophore (purple). The cell-permeable antagonist is conjugated with a Cy5 dye. (*C*) Computational analysis of the binding interaction between cell-permeable antagonist and β1AR (PDB:7BTS). (*D*) β1AR orthosteric pocket and pharmacophore interaction sites. D1138 and F1218 are β1AR residues interacting with the pharmacophore via H-bond an π-cation interaction, respectively.

To find a suitable βAR antagonist that only inhibits the plasma membrane pool of the receptor, we analyzed the structure–activity relationships of existing antagonists. We found that multiple existing β-blockers (i.e., metoprolol, bisoprolol, and flusoxolol) share the same core pharmacophore but differ in their substituents in para-position of the aromatic ring (*SI Appendix*, Fig. S3*A*) (38, 39). Thus, we decided to attach a linker on the aromatic ring to conjugate cyanine5 (Cy5) or impermeable sulfo-cyanine5, resulting in a pair of permeable and impermeable antagonist for βARs (Fig. 2 *A* and *B*). The choice of a Cy5 dye with or without a sulfonate provides not only a means to restrict membrane permeability but a fluorescent dye to directly image the location of both pharmacological agents. To obtain these molecules, an alkyne intermediate was generated in three synthetic steps from tyramine and 4-pentynoic acid and was subsequently coupled with azido-functionalized fluorophores using click chemistry (*SI Appendix*). To test whether these functionalized ligands are indeed binding β1AR as exemplary βARs, we conducted docking studies with PDB 7BTS (40). We obtained a docking score of −10.581 for poses in which the pharmacophore is engaging the orthosteric binding site through the interaction with two key residues (D1138 and F1218) and the conjugated fluorophore extends out of the binding pocket (Fig. 2 *C* and *D* and *SI Appendix*, Fig. S3*B*). These data suggest that the conjugated cell-permeable and -impermeable antagonists can engage β1AR similar to previously reported β1AR antagonists.

Characterization of Spatially Restricted βAR Antagonists. To assess whether our newly designed βAR antagonists' function in a spatially restricted manner, we first checked their cellular distributions. Given that these antagonists are conjugated to a sulfonated or nonsulfonated Cy5, they are intrinsically fluorescent and thus can be visualized by live imaging. We found that while cell-permeable βAR antagonist rapidly accumulates inside the cells, the cell-impermeable antagonist is unable to cross the plasma membrane and remains outside the cells (*SI Appendix*, Fig. S4 *A* and *B*). We next determined the pharmacological properties of these antagonists. Both antagonists have similar efficacy and potency, as measured by their inhibitory effect on βARs-mediated cAMP response for β1AR, β2AR, and β3AR (Fig. 3 *A* and *B*, *SI Appendix*, Fig. S5 *A*–*C*, and Datasets S4 and S5). Having determined the most effective concentrations (10 μM), we then tested their ability to inhibit compartmentalized β1AR signaling, using our nanobody-based biosensor. HeLa cells expressing SNAP-tagged β1AR and Nb80-GFP were stimulated with 1 μM dobutamine for 15 min. Dobutamine is a cell-permeable β1AR agonist and activates both the plasma membrane and the Golgi pool of β1AR, as demonstrated by Nb80-GFP recruitment to both locations (Fig. 3 *C*, *Upper*). We then added 10 μM of the nonselective cell-impermeable antagonist and noticed that while Nb80-GFP was still associated with the Golgi membranes, its localization to the plasma membrane was lost, suggesting that only the plasma membrane-β1AR is inhibited (Fig. 3 *C*, *Lower* and Fig. 3*D* and Dataset S6). In contrast, the cell-permeable antagonist inhibits β1ARs at the plasma membrane and the Golgi and thus promotes Nb80-GFP dissociation from both compartments (Fig. 3 *E* and *F*, and Dataset S7). Given that both drugs have comparable potencies and efficacies, these data suggest that the sulfonated chemical group makes the antagonist cell impermeable, thus only inhibiting plasma membrane–localized β1AR.

Cell-Impermeable βAR Antagonist Blocks β1AR Signaling on the Plasma Membrane in ACM. In cardiomyocytes, β1AR-mediated cAMP generation regulates heart rate, force of contraction, and relaxation through PKA-mediated phosphorylation of proteins, such as TnI, RyR2, and PLB (Fig. 4*A*) (35). We have recently demonstrated that activation of the plasma membrane–localized β1ARs promotes PKA-mediated phosphorylation of TnI and RyR2. In contrast, the Golgi-β1AR signaling specifically phosphorylates PLB (33). To functionally test the compartment-specific inhibitory effects of our newly designed antagonists, we next assessed the phosphorylation status of downstream effectors of PKA upon β1AR activation. We specifically measured RyR2 and PLB phosphorylation, as readouts of the plasma membrane and Golgi-localized β1AR signaling, respectively. Treatment of ACMs with cell-permeable βAR antagonist resulted in the inhibition of both RyR2 and PLB phosphorylation upon epinephrine stimulation (Fig. 4 *B* and *C*, and Dataset S8). Importantly, treatment of ACMs with cell-impermeable βAR antagonist, only blocked RyR2 phosphorylation, while PLB phosphorylation was not affected (Fig. 4 *B* and *C*, and Dataset S8).

Given that β1AR-mediated phosphorylation of RyR2 and PLB accelerates sarcoplasmic reticulum (SR) Ca^{2+} release and reuptake, respectively, we evaluated the effects of permeable and impermeable antagonists on Ca^{2+} transient using optical mapping on freshly isolated ACMs. The Ca^{2+} release phase was characterized by the parameter time to peak (TTP), and the Ca^{2+} reuptake phase was characterized by the parameter time from Ca^{2+} transient peak to 50% relaxation (T50) and decay constant (Tau) (Fig. 4*D*). Epinephrine stimulation significantly shortened TTP compared to the baseline group, primarily due to the phosphorylation of RyR2 during the excitation–contraction coupling. This effect was abolished by the application of both permeable and impermeable antagonists (Fig. 4*E* and Dataset S9). This suggests that the enhancement of SR Ca^{2+} release upon epinephrine stimulation was blocked by both antagonists. During the reuptake phase, the permeable antagonist significantly prolonged T50 and Tau to the

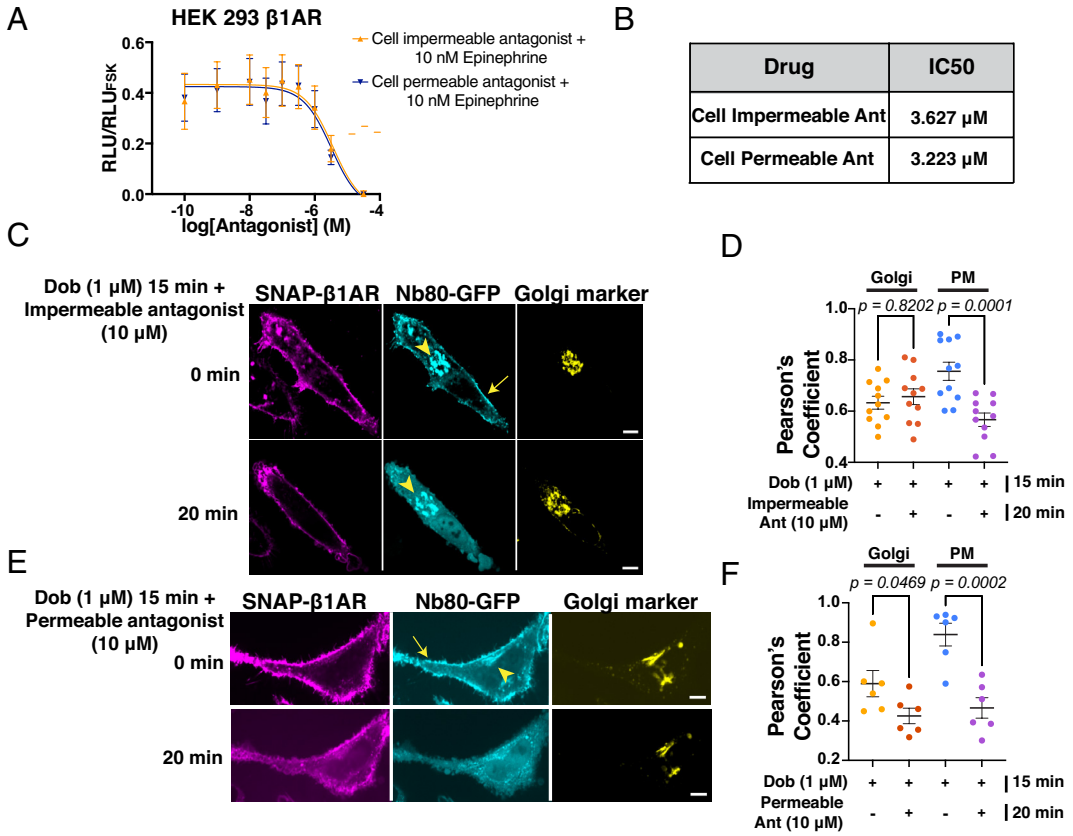

Fig. 3. Conformational biosensor, Nb80-GFP, detects activated β1AR before and after cell-permeable or -impermeable antagonists' treatment. (*A*) Concentration–response curve of the cell-permeable (blue line) and the cell-impermeable (orange line) antagonists in HEK293 overexpressing β1AR and a bioluminescent cAMP biosensor. Cells were treated with different concentrations of antagonists in combination with ~10 nM epinephrine. Relative luminescence values are normalized to HEK293 cells treated with forskolin (20 μM). n = 4 independent biological replicates. (*B*) IC50 values of cell-impermeable and -permeable antagonist are respectively 3.627 μM and 3.223 μM. (*C*) Confocal images of representative HeLa cells expressing Nb80-GFP (cyan) and SNAP-β1AR (SNAP surface staining, magenta) and the Golgi marker (yellow), pretreated with dobutamine (1 μM) for 15 min. Stimulation with cell-impermeable antagonist (10 μM) for 20 min selectively inhibits the plasma membrane-localized β1AR. The arrow indicates the plasma membrane, and arrowheads indicate Golgi localization. (Scale bar: 10 μm.) (*D*) Person's correlation coefficient measurements for the colocalization analysis of Nb80-GFP at the Golgi and plasma membrane after treatments of cardiomyocytes with the cell-impermeable antagonist. The results have been measured from n = 10 cells, three independent biological replicates; *P* values were calculated by one-way ANOVA. (*E*) Confocal images of representative HeLa cells expressing Nb80-GFP (cyan) and SNAP-β1AR (SNAP surface staining, magenta) and the Golgi marker (yellow), pretreated with dobutamine (1 μM) for 15 min. Stimulation with cell-permeable antagonist (10 μM) for 20 min inhibits both the plasma membrane and the Golgi pool of β1AR. The arrow indicates the plasma membrane, and arrowheads indicate Golgi localization. (Scale bar: 10 μm.) (*F*) Person's correlation coefficient measurements for the colocalization analysis of Nb80-GFP at the Golgi and plasma membrane for cardiomyocytes treated with the cell-permeable antagonist. The results have been measured from n = 6 cells, two independent biological replicates; *P*-values were calculated by one-way ANOVA.

level of the baseline group. In contrast, the impermeable antagonist did not affect these parameters, with values similar to the epinephrine-treated group (Fig. 4*E* and Dataset S9). These findings suggest that permeable antagonist, but not impermeable antagonist, blocks the epinephrine-induced PLB/SERCA-mediate acceleration of Ca^{2+} reuptake. These data further confirm the selective inhibitory effect of these compartment-specific antagonists on specific downstream effectors of βARs, thereby regulating distinct cellular and physiological responses.

Discussion

In this study, we report the development of β-blockers that are spatially restricted and can be used to manipulate βAR compartmentalized signaling across cell types and tissues. By conjugating the pharmacophore of known β-blockers to a sulfonated fluorophore, we generated a membrane-impermeable βAR antagonist. By comparing the membrane-impermeable βAR antagonist to the cell-permeable version of the same drug with similar potency and efficacy, we further show the functional significance of their effect in regulating β1AR-mediated signaling in cardiomyocytes. The cell-impermeable antagonist only inhibited β1AR and downstream effectors of PKA proximal to the plasma membrane while β1AR Golgi pool remained active, demonstrated through continued epinephrine-induced PLB phosphorylation and accelerated Ca^{2+} reuptake (Fig. 4). In contrast, cell-permeable βAR antagonist efficiently inhibit both the plasma membrane and Golgi pools of β1ARs. We believe that this strategy allows for direct interrogation of compartmentalized βAR signaling particularly for assessing their biological functions in cardiomyocytes. It can also be potentially employed to manipulate several other GPCRs in a compartment-specific manner.

In a recent study, a positive correlation between lipophilicity, based on the calculated logP values of chemically modified serotonin ligands, and their psychoplastogenic effects was reported (41). The modification of GPCR agonists or antagonists with sulfonate groups has been previously used to visualize the distribution of receptors on the cell surface (42). For example, a sulfonated and fluorescently labeled analogue of an inverse βAR agonist, carazolol, or high-affinity agonist BI-167107 has been used to detect the distributions and dynamics of β1AR and β2AR on the plasma membrane (43, 44). However, none of these modified drugs were used to resolve the spatial functions of βARs. Our present study reports direct assessment of such chemical modifications and their consequent effects on cellular responses mediated by β1AR signaling in cardiomyocytes.

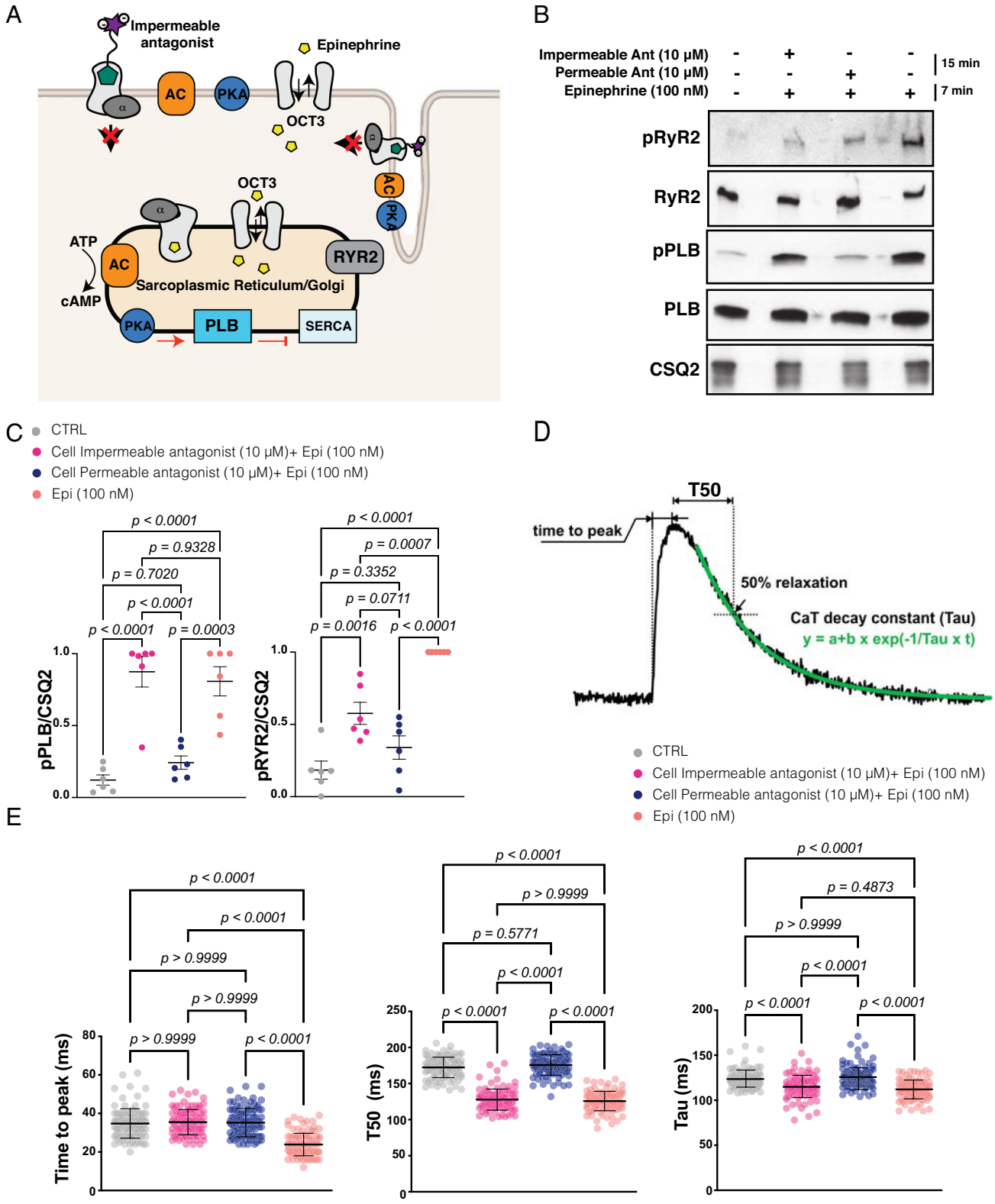

Fig. 4. Cell-impermeable antagonist only inhibits β1AR-mediated responses from the plasma membrane. (*A*) Illustration of the effect of membrane-impermeable antagonist in blocking β1AR-mediated signaling in ACM. (*B*) Representative phosphorylation profiles of RyR2 and PLB induced by epinephrine (100 nM) alone, or in combination with the cell-impermeable and -permeable antagonists (10 μM) in ACM. Phosphorylation of RyR2 Ser2808 (pRyR2) and PLB Ser16/Thr17 (pPLB) was analyzed in wild-type ACMs endogenously expressing β1AR by immunoblotting. (*C*) Quantification of immunoblots of pPLB and pRYR2 was normalized to the protein levels of CSQ2 and then reported as a percentage of the highest value in the groups. The quantified data from different experiments are presented as mean ± SEM. The *P*-values were calculated by two-way ANOVA. n = 6 independent biological replicates. (*D*) Representative Ca^{2+} transient trace analysis. (*E*) Comprehensive quantification and comparison of time to peak (TTP), T50, and decay constant (Tau) from the four groups. N = 100 cells per condition in n = 3 independent biological replicates. One-way ANOVA was used to compare the parameters with the post hoc test using Bonferroni's multiple comparison test. The data are presented as mean± SD.

Other approaches to manipulate intracellular GPCR signaling take advantage of chemically modified agonists and antagonists that are inactive until light-induced uncaging of active ligands (45–49). While this approach has been used to temporally control GPCR activity, spatial control has mainly been applied to map synaptic connectivity in neuronal networks (48). There are few studies that have utilized caged compounds to manipulate spatial GPCR signaling at the subcellular level. For example, a caged cell-permeable analog of the endothelin B antagonist was shown to specifically block intracellular endothelin receptors signaling (50). Another report on angiotensin II receptors, took advantage of a caged version of Ang-II to demonstrate receptor signaling from intracellular compartments (49). We have previously used caged dopamine to activate D1DR signaling at the Golgi (11). While caged ligands can be useful to study subcellular GPCR activity in cells, they have some shortcomings for in vivo studies. For example, limited light penetration in tissues and in some cases the side products of photolysis can create unintended consequences (48). Moreover, many uncaged ligands can passively diffuse or be transported out of the cells via the same transport mechanism that facilitates their transport inside the cells. This is a particularly significant issue for caged monoamines (i.e., dopamine, epinephrine) that are transported by organic cation transporters (OCTs), known to function in a bidirectional manner (30). Thus, uncaged monoamines can be transported in and out of the cells over time and activate both pools of monoamine GPCRs (11). For example, we have previously demonstrated that epinephrine, an endogenous/hydrophilic βAR agonist, requires a facilitated transport via an organic cation transporter, OCT3, to reach the β1ARs at the Golgi (9, 23, 33). Similarly, we found that OCT2 facilitates the transport of dopamine to activate D1 dopamine receptor signaling at the Golgi (11). Thus, in cells expressing OCT3 or OCT2, uncaged epinephrine/norepinephrine or dopamine can be transported in and out of the cell via OCT3 or OCT2, respectively. This complexity makes the interpretation of the biological responses more complicated.

The complexity and variable tissue expression patterns of cation or anion transporters limit the utility of currently available GPCR drugs for studying their spatial function (30, 32). As reported in this study, sotalol, a relatively hydrophilic βAR antagonist can cross the membrane in an OATP1A2-dependent fashion. We found that in HeLa cells sotalol cannot cross the membrane and can only inhibit the plasma membrane-localized β1ARs. Other studies in rat-derived cardiomyocytes have also reported similar effect for sotalol treatments (23, 51). In contrast, ACM derived from mice express OATP1A2, thus sotalol can be transported into the cell and inhibit both the plasma membrane and the Golgi pool of β1ARs. Several factors could contribute to varying impact of sotalol across different cell types. These include changes in the extracellular pH, the presence of scaffolding proteins, and post-translational modifications, all of which can impact the surface and subcellular localization as well as the function of OATP1A2 (52–55). The use of sulfonated GPCR agonist and antagonist particularly for monoamine GPCRs therefore offers the critical advantage to restrict drug access to subcellular compartments across cell types and tissues. The described strategy could be broadly applicable to modify other GPCR agonists and antagonists to resolve subcellular signaling profiles. It could further be useful in the clinical studies to distinguish between desired and undesired effects in therapy.

Materials and Methods

Reagents and Antibodies. Human insulin, human transferrin, and sodium selenite (ITS); urethane; 2,3-butanedione monoxime (BDM); Taurine; protease XIV; polybrene; forskolin (FSK); epinephrine; dobutamine; sotalol; metoprolol; and naringin are from Sigma; and salmeterol and CL-316243 are from Abcam. Glutamax solution, penicillin and streptomycin, 4-(2-hydroxyethyl)-1-piperazineethanesulfonic acid (HEPES) buffer, DMEM, DMEM F12, M199 medium, Hanks' Balanced Salt Solution (HBSS) buffer, ultrapure H_2O, mouse laminin, and Halt protease and phosphatase inhibitor cocktail are from Thermo Fisher Scientific. Fetal bovine serum (FBS) and Nu-Serum IV are from Corning. Glucose, sodium phosphate monobasic monohydrate, sodium chloride, potassium chloride, magnesium chloride hexahydrate, Tris–base, ethylenediaminetetraacetic acid (EDTA), dithiothreitol (DTT), dimethyl sulfoxide, Tween 20, and HEPES are from Fisher Bioreagents. Doxycycline is from Takara. Calcium chloride is from Acros Organics. ICI-118551 is from Tocris Bioscience. Collagenase II is from Worthington. Bovine serum albumin (BSA) and dry milk powder are from Research Products International. SNAP-Surface Alexa Fluor 546 (S9132S), SNAP-Cell TMR-Star (S9105S), and SNAP-Cell 647 SiR (S9102S) are from New England Biolabs. Heparin solution is from Fresenius Kabi. Triton X-100 is from Bio-Rad. Rabbit anti-phospho PLB (Ser16/Thr17) antibody (8496), rabbit anti-PLB antibody (4562S), and rabbit anti-phospho TnI (Ser23/Ser24) antibody (4004) are from Cell Signaling. Rabbit anti-phospho ryanodine receptor 2 (Ser2808) antibody (PA5-104444) is from Thermo Fisher Scientific. Rabbit anti-calsequestrin 2 (CSQ2) antibody (18422-1-AP) and rabbit anti-ryanodine receptor 2 (19765-1-AP) are from Proteintech, rabbit anti-OATP1A2 antibody (ab221804) is from Abcam, mouse anti-a-Actinin antibody (7811) is from Sigma, and sheep anti-TGN38 antibody (AHP499G) is from Bio-Rad. Amersham ECL donkey anti-rabbit IgG (NA934V) and horseradish peroxidase-linked whole antibodies were purchased from GE Healthcare Life Sciences.

General Method for Spatially Restricted Antagonist Synthesis. Anhydrous solvents were purchased from Acros Organics. Unless specified below, all chemical reagents were purchased from Sigma-Aldrich, Oakwood, Ambeed, or Chemscene. Analytical thin layer chromatography (TLC) was performed using aluminum plates precoated with silica gel (0.25- mm, 60-Å pore size, 230 to 400 mesh, Merck KGA) impregnated with a fluorescent indicator (254 nm). TLC plates were visualized by exposure to ultraviolet light (UV). Flash column chromatography was performed with the Teledyne ISCO CombiFlash EZ Prep chromatography system, employing prepacked silica gel cartridges (Teledyne ISCO RediSep). Proton NMR (1H NMR) spectra were recorded on the Bruker Avance III HD instrument (400 MHz/100 MHz/376 MHz) at 23 °C operating with the Bruker Topspin 3.1. NMR spectra were processed using Mestrenova (version 14.1.2). Proton chemical shifts are expressed in parts per million (ppm, δ scale) and are referenced to residual protium in the NMR solvent (CHCl3: δ 7.26, MeOD: δ 3.31). Data are represented as follows: chemical shift, multiplicity (s = singlet, d = doublet, t = triplet, q = quartet, dd = doublet of doublets, dt = doublet of triplets, m = multiplet, br = broad, app = apparent), integration, and coupling constant (J) in Hertz (Hz). High-resolution mass spectra were obtained using a Waters Xevo G2-XS time-of-flight mass spectrometer operating with Waters MassLynx software (version 4.2). When LC–MS analysis of the reaction mixture is indicated in the procedure, it was performed as follows. An aliquot (1 μL) of the reaction mixture (or the organic phase of a mini-workup mixture) was diluted with 100 μL 1:1 acetonitrile/water. 1 μL of the diluted solution was injected onto a Waters Acquity UPLC BEH C18 1.7 μm column and eluted with a linear gradient of 5 to 95% acetonitrile/water (+0.1% formic acid) over 3.0 min. Chromatograms were recorded with a UV detector set at 254 nm and a time-of-flight mass spectrometer (Waters Xevo G2-XS).

Computational Modeling. The β1-AR structure from 7BTS was prepared using the Protein Preparation Wizard tool in Maestro (Schrödinger Suite 2023-1, Schrödinger, LLC, New York), and parts of the lysozyme were removed. The ligand was prepared using the LigPrep tool and docked into the protein using Glide. A truncated version without fluorophore was docked initially and then used as a reference ligand to dock the full ligand. The resulting docking scores were −7.658 for the truncated and −10.581 for the full ligand.

Cell Culture and Lentivirus Production. HeLa, HE293T, and HEK 293 cells are cultured in DMEM with 10% FBS. HEK293T were cotransfected with pMD2.G, pSPAX2, and Nb80-GFP and SNAP-β1AR plasmids using as transfection reagent TransIT-Lenti (mir6600, Mirus bio). Lentivirus was produced in DMEM containing

10% FBS and 1% BSA and then concentrated using the Lenti-X concentrator (Takara Bio).

Animals. CD1 and C57BL/6 WT mice were housed in the UCSF facilities controlled by standardized environmental parameters such as 12 h light/12 h dark cycle in 7 d per week, humidity 30 to 70%, temperature 20 to 26 °C, and constant access to water and foods. All animal experiments were approved by the Institutional of Animal Care and Use Committee of the University of California, San Francisco.

Primary Culture of NCMs. Hearts collected from P1–2 neonatal CD1 pups were cut into small pieces in ice-cold HBSS containing 20 mM HEPES. Heart pieces mixed with 225 IU ml^{-1} collagenase II were incubated on a rotator at 37 °C for 5 min. After several pipetting, the released cells in the buffer were collected by centrifuge at 500 g for 5 min. The undigested heart tissues were digested again, as described above, until the undigested tissue became white The cells from each digestion were pooled together and resuspended in the NCM culture media, which is DMEM containing 10% FBS, 10% Nu-Serum IV, 10 mM HEPES, ITS, 10 mM GlutaMAX, penicillin, and streptomycin. The isolated cells are passed through a 40 μm strainer and plated in a regular petri dish to remove the most of fibroblasts at 37 °C for 2 h. The fibroblast supernatant containing NCMs was collected and plated on mouse laminin-coated imaging dishes. For the virus transduction, lentivirus was mixed with the culture media with polybrene (8 μg ml^{-1}). Virus was removed after 1-d transduction. The transduced NCMs were further treated with doxycycline for 3 d.

Primary Culture of ACM. ACM were isolated from 2- to 3-mo-old C57BL/6 WT male mice using the Langendorff-free method (56). We intraperitoneally injected heparin solution into the mouse (5 U g^{-1}). After 10 min, urethane, dissolved in 0.9% NaCl, was also intraperitoneally injected into the mouse (2 mg g^{-1}). Once the mouse was anesthetized, we exposed the heart, and the inferior vena cava was cut to release the blood. First, EDTA buffer (130 mM NaCl, 5 mM KCl, 0.5 mM NaH_2PO_4-H_2O, 10 mM HEPES, 10 mM glucose, 10 mM BDM, and 10 mM Taurine, in ultrapure H_2O, pH 7.8) was injected into the right ventricle, and subsequently, the aorta was clamped. The clamped heart was moved to the EDTA buffer-containing dish, and then, the EDTA buffer was injected into the left ventricle. Then, the clamped heart was moved to the perfusion buffer (130 mM NaCl, 5 mM KCl, 0.5 mM NaH_2PO_4–H_2O, 10 mM HEPES, 10 mM glucose, 10 mM BDM, 10 mM Taurine, and 1 mM $MgCl_2$–$6H_2O$, in ultrapure H2O, pH 7.8) containing dish, and the perfusion buffer was injected into the left ventricle. The clamped heart was further moved to the digestion buffer (perfusion buffer with 1 mg ml^{-1} collagenase II and 0.05 mg ml^{-1} protease XIV) containing dish, and then, the digestion buffer was injected into the left ventricle. After digestion, the heart was cut into small pieces and gently triturated to dissociate the cardiomyocytes. The digestion processes were stopped by adding stop buffer (perfusion buffer with 10% FBS), and the suspended cardiomyocytes were passed through a 100 μm strainer. The cardiomyocytes were enriched by gravity sedimentation and reintroduced calcium gradually. We resuspended the cardiomyocytes in plating media (M199 media with 5% FBS, 10 mM BDM, penicillin, and streptomycin) and seeded on mouse laminin-coated wells at 37 °C for 1 h. After washing out the unattached cells by culture media (M199 media with 0.1% BSA, 10 mM BDM, penicillin and streptomycin, and ITS), the cardiomyocytes were cultured in culture media for the drug treatment.

Luminescence-Based cAMP Assay. HEK293 cells were transfected with β1AR or β2AR or β3AR and a cyclic-permuted luciferase reporter construct (pGloSensor-20F, Promega), and luminescence values were measured, as described previously (6). Briefly, cells were plated in 96-well dishes (~100,000 cells per well) in DMEM F12 without phenol red/no serum (21041-025, ThermoFisher) and equilibrated to 37 °C in the SpectraMax plate reader, and luminescence was measured every 2 min for 20 min. Software was used to calculate integrated luminescence intensity and background subtraction. The agonist experiments have been carried out adding different concentrations of epinephrine (1237000, Sigma) and dobutamine (D0676, Sigma). The antagonist experiments (cell-permeable and -impermeable spatially selective antagonists, sotalol (S0278, Sigma) and metoprolol (21041, Sigma) have been carried out incubating the cells at 37 °C for 30 min. Cells were stimulated using the previously calculated EC80 of epinephrine (1237000), dobutamine (D0676), salmeterol (AB120771-1001), and CL-316243 (ab144605). 20 μM FSK (F6885, Sigma) was used as a reference value in each multiwell plate and for each experimental condition. The average luminescence value (measured across triplicate wells) was normalized to the maximum luminescence value measured in the presence of 20 μM FSK (F6885, Sigma).

Live-Cell Confocal Imaging. Live-cell imaging was carried out using a Nikon spinning disk confocal microscope with a ×60, 1.4 numerical aperture, oil objective, and a CO_2 and 37 °C temperature-controlled incubator. A 406, 488, 568, and 640 nm Voltran was used as light sources for imaging mTagBFP2, GFP, SNAP-Surface Alexa Fluor 546, SNAP-Cell TMR-Star, and SNAP-Cell 647 SiR signals, respectively. In the experiments conducted in HeLa cells, cells expressing SNAP-tagged β1AR and β2AR receptor, Nb80-GFP, and GalT-mTagBFP2 (Golgi marker) were imaged in 35 mm bottom glass imaging dishes. Receptors were surface labeled by addition of SNAP-Surface Alexa Fluor 546 (1:1,000, New England Biolabs) to DMEM F12 without serum and phenol red (21041-025, ThermoFisher) supplemented with 30 mM HEPES pH 7.4 (15630080, ThermoFisher) for 10 min. Live-cell images where we tested the effect of the spatially restricted antagonist in HeLa β1AR overexpressing cells were carried out by incubating the cells in 1 μM dobutamine (D0676, Sigma) at 37 °C for 20 min before indicated spatially selective antagonists were added. Live-cell images where we tested the effect of the spatially restricted antagonist in HeLa β2AR overexpressing cells were carried out by incubating the cells in 100 nM epinephrine (1237000, Sigma) at 37 °C for 10 min before indicated spatially selective antagonists were added. Cells were imaged before and after 15 min from antagonist addition. Time-lapse images were acquired with a CMOS camera (Photometrics) driven by Nikon Imaging Software (NS Elements). In the experiments conducted in mouse NCM, cells were isolated from neonatal CD1 mice and infected with pLVX-TetOne-SNAP-β1AR and pUBC-Nb80-GFP lentivirus as previously described. Cell expressing both SNAP-β1AR and Nb80-GFP were imaged in 35 mm bottom glass imaging dishes. Receptors were labeled both at the surface and intracellularly by the cell-permeable SNAP-Cell 647 SiR ligand (1:1,000, New England Biolabs) in DMEM F12 without serum and phenol red (21041-025, ThermoFisher) supplemented with 30 mM HEPES pH 7.4 (15630080, ThermoFisher) for 20 min. Live-cell images of NCM stimulated with dobutamine had been carried out by imaging cells before the addiction of 10 μM dobutamine. After 5 min from the addiction of dobutamine, 100 μM sotalol (S0278, Sigma) was added to the cells. Cells were imaged every 10 s for 15 min. Time-lapse images were acquired with a CMOS camera (Photometrics) driven by Nikon Imaging Software (NS Elements).

Fixed-Cell Confocal Imaging. ACM isolated from wild-type mice were fixed with 4% paraformaldehyde directly added to ACMs in culture media for 10 min and quenched with 50 mM NH4Cl in PBS for 15 min. ACMs were permeabilized with 0.1% Triton X-100 and blocked with 2.5% BSA in PBS for 20 min. Primary antibodies against OATP1A2 antibody (ab221804) (1:50) were incubated with or without its blocking peptide (1:100) in 0.1%/2.5%BSA solution. The blocking peptide was custom synthesized using the peptide sequence fragment corresponding to human OATP1A2 aa 250–350, Uniprot ID: P46721) and diluted in water at a concentration of 1 mg/mL.

Antibodies raised against TGN 38 (AHP499G) (1:200) and a-Actinin (7 811) (1:500) with or without OATP1A2 blocking peptide (Elimbio) were diluted in 0.1% Triton X-100 and 2.5% BSA solution. Confocal images were taken using a Nikon spinning disk confocal microscope with a 60 × 1.4 numerical aperture and oil immersion objective.

Image Analysis and Statistical Analysis. Images were saved as 16-bit TIFF files. Quantitative image analysis was carried out on unprocessed images using ImageJ (http://rsb.info.nih.gov/ij). Analysis of Nb80-GFP colocalization analysis at the plasma membrane and Golgi in HeLa cells was estimated after background subtraction by calculating the Pearson's coefficient between the indicated image channels with the plasma membrane marker (Surface SNAP-β1AR) and Golgi marker channel (GalT-mTagBFP2), using the colocalization the plugin for ImageJ JaCoP (57). For visual presentation (but not quantitative analysis), image series were processed using Kalman stack filter in ImageJ. *P* values are determined using two-way ANOVA calculated with Prism 10.0 software (GraphPad Software).

Ca^{2+} Transient Optical Mapping of Isolated Ventricular Myocytes. Optical mapping of Ca^{2+} transients was conducted as previously described. Briefly, freshly isolated ventricular myocytes were incubated with the Ca^{2+} probe Fluo-4 AM (10 μmol/L) for 15 min and then washed twice with Tyrode solution for another

20 min to allow the sufficient intracellular de-esterification (58). The cells were then excited at 488 nm, and the emitted fluorescence signals were collected through a 520 nm filter during 2 Hz field stimulation. The experiment was performed using an inverted Nikon fluorescent microscope (Eclipse Ti) equipped with a MiCAM Ultima-L CMOS camera (SciMedia, USA Ltd., CA). The sampling frequency is 500 to 1,000 frames/s. The signals were analyzed using a custom-made Matlab-based algorithm. Ca^{2+} transient time to peak (TTP), T50 (time from Ca^{2+} transient peak to 50% relaxation), and decay constant (Tau) were measured (59). These parameters were assessed and compared among four groups of cells: cells at baseline condition; cells treated with epinephrine; cells treated with epinephrine and permeable antagonist; and cells treated with epinephrine and impermeable antagonist.

Western Blotting. After drug treatments, the cardiomyocytes adult mice were collected and lysed by RIPA buffer containing inhibitors of proteases and phosphatases at 4 °C for 30 min. Supernatants were collected after centrifuging at 4 °C for 10 min, and the protein amounts were determined by BCA assay (Sigma). The proteins were reduced and denatured by boiling for 10 min in sample buffer with DTT, separated by 4 to 20% Mini-PROTEIN TGX gels (Bio-Rad) and transferred to the 0.2 µm polyvinylidene difluoride (PVDF) membrane (Bio-Rad). The membrane was then blocked by TBST (TBS buffer with 0.1% Tween 20) buffer containing 3% milk at room temperature for 1 h and then incubated with the primary antibody in TBST with 5% BSA at 4 °C for O/N in the case of pRYR2, profile of PLB, CSQ2, and OATP1A2 and 1 h at room temperature for RYR2 and PLB. The PVDF membrane was washed with TBST and incubated with a secondary antibody diluted in TBST containing 3% milk at room temperature for 1 h. The unbonded secondary antibodies were removed by TBST wash. The protein signals were visualized by ECL substrate (34580, ThermoFisher). To evaluate the relative band intensities, we first scanned our films (300 ppi resolution) using an office scanner and convert them to an 8-bit format. We then inverted these images and subtracted the background using ImageJ software. The bands were selected using the rectangular selection tool on ImageJ. The relative band intensities were plot and measured; each peak was separated by straight-line selection tool. The area of each peak was measured using the Wand tool. Semiquantified phosphoprotein bands were then normalized to the total lysate bands (CSQ2), and data were presented as fold change of the maximum value that we measured on each western blot. *P* values are determined using two-way ANOVA calculated with Prism 10.0 software (GraphPad Software).

Data, Materials, and Software Availability. All study data are included in the article and/or supporting information.

ACKNOWLEDGMENTS. We thank members of the Irannejad and the Shokat Labs for their assistance, advice, and valuable discussion. We also thank The Center for Advance Imaging for helping with the biosensor imaging assay and analysis at University of California, San Francisco. These studies were supported by the National Institute of General Medicine (GM133521 to R.I.), the Sandler Program for Breakthrough Biomedical Research (PBBR7031249 to F.L.), the National Cancer Institute (K99CA277358 to J.M.), and (5R01CA244550 to K.M.S).

Author affiliations: [a]Cardiovascular Research Institute, Department of Biochemistry & Biophysics, University of California, San Francisco, CA 94143; [b]Department of Biochemistry & Biophysics, University of California, San Francisco, CA 94143; [c]Department of Cellular and Molecular Pharmacology, University of California, San Francisco, CA 94143; and [d]HHMI, University of California, San Francisco, CA 94143

Author contributions: F.L., J.M., K.M.S., and R.I. designed research; F.L., J.M., T.-Y.L., J.P., and D.L. performed research; J.M. contributed new reagents/analytic tools; F.L. and T.-Y.L. analyzed data; and F.L., J.M., K.M.S., and R.I. wrote the paper.

1. K. L. Pierce, R. T. Premont, R. J. Lefkowitz, Seven-transmembrane receptors. *Nat. Rev. Mol. Cell Biol.* **3**, 639–650 (2002).
2. D. Calebiro *et al.*, Persistent cAMP-signals triggered by internalized G-protein-coupled receptors. *PLoS Biol.* **7**, e1000172 (2009).
3. T. N. Feinstein *et al.*, Noncanonical control of vasopressin receptor type 2 signaling by retromer and arrestin. *J. Biol. Chem.* **288**, 27849–27860 (2013).
4. S. Ferrandon *et al.*, Sustained cyclic AMP production by parathyroid hormone receptor endocytosis. *Nat. Chem. Biol.* **5**, 734–742 (2009).
5. S. J. Kotowski, F. W. Hopf, T. Seif, A. Bonci, M. von Zastrow, Endocytosis promotes rapid dopaminergic signaling. *Neuron* **71**, 278–290 (2011).
6. R. Irannejad *et al.*, Conformational biosensors reveal GPCR signalling from endosomes. *Nature* **495**, 534–538 (2013).
7. N. G. Tsvetanova, M. von Zastrow, Spatial encoding of cyclic AMP signaling specificity by GPCR endocytosis. *Nat. Chem. Biol.* **10**, 1061–1065 (2014).
8. N. G. Tsvetanova *et al.*, Endosomal cAMP production broadly impacts the cellular phosphoproteome. *J. Biol. Chem.* **297**, 100907 (2021).
9. R. Irannejad *et al.*, Functional selectivity of GPCR-directed drug action through location bias. *Nat. Chem. Biol.* **13**, 799–806 (2017).
10. A. Godbole, S. Lyga, M. J. Lohse, D. Calebiro, Internalized TSH receptors en route to the TGN induce local Gs-protein signaling and gene transcription. *Nat. Commun.* **8**, 443 (2017).
11. N. M. Puri, G. R. Romano, T. Y. Lin, Q. N. Mai, R. Irannejad, The organic cation Transporter 2 regulates dopamine D1 receptor signaling at the Golgi apparatus. *Elife* **11**, e75468 (2022).
12. M. J. Lohse, A. Bock, M. Zaccolo, G protein-coupled receptor signaling: New insights define cellular nanodomains. *Annu. Rev. Pharmacol. Toxicol.* **64**, 387–415 (2023), 10.1146/annurev-pharmtox-040623-115054.
13. D. D. Jensen *et al.*, Neurokinin 1 receptor signaling in endosomes mediates sustained nociception and is a viable therapeutic target for prolonged pain relief. *Sci. Transl. Med.* **9**, eaal3447 (2017).
14. R. E. Yarwood *et al.*, Endosomal signaling of the receptor for calcitonin gene-related peptide mediates pain transmission. *Proc. Natl. Acad. Sci. U.S.A.* **114**, 12309–12314 (2017).
15. N. N. Jimenez-Vargas *et al.*, Protease-activated receptor-2 in endosomes signals persistent pain of irritable bowel syndrome. *Proc. Natl. Acad. Sci. U.S.A.* **115**, E7438–E7447 (2018).
16. P. D. Ramirez-Garcia, N. A. Veldhuis, N. W. Bunnett, T. P. Davis, Targeting endosomal receptors, a new direction for polymers in nanomedicine. *J. Mater. Chem. B* **11**, 5390–5399 (2023).
17. M. von Zastrow, A. Sorkin, Mechanisms for regulating and organizing receptor signaling by endocytosis. *Annu. Rev. Biochem.* **90**, 709–737 (2021).
18. D. P. Poole, N. W. Bunnett, G protein-coupled receptor trafficking and signalling in the enteric nervous system: The past, present and future. *Adv. Exp. Med. Biol.* **891**, 145–152 (2016).
19. P. D. Ramirez-Garcia *et al.*, A pH-responsive nanoparticle targets the neurokinin 1 receptor in endosomes to prevent chronic pain. *Nat. Nanotechnol.* **14**, 1150–1159 (2019).
20. N. N. Jimenez-Vargas *et al.*, Endosomal signaling of delta opioid receptors is an endogenous mechanism and therapeutic target for relief from inflammatory pain. *Proc. Natl. Acad. Sci. U.S.A.* **117**, 15281–15292 (2020).
21. S. G. Rasmussen *et al.*, Structure of a nanobody-stabilized active state of the beta(2) adrenoceptor. *Nature* **469**, 175–180 (2011).
22. A. M. Ring *et al.*, Adrenaline-activated structure of beta2-adrenoceptor stabilized by an engineered nanobody. *Nature* **502**, 575–579 (2013).
23. C. A. Nash, W. Wei, R. Irannejad, A. V. Smrcka, Golgi localized beta1-adrenergic receptors stimulate Golgi PI4P hydrolysis by PLCepsilon to regulate cardiac hypertrophy. *Elife* **8**, e48167 (2019).
24. S. C. Wright *et al.*, BRET-based effector membrane translocation assay monitors GPCR-promoted and endocytosis-mediated G(q) activation at early endosomes. *Proc. Natl. Acad. Sci. U.S.A.* **118**, e2025846118 (2021).
25. D. J. Marcus, M. R. Bruchas, Optical approaches for investigating neuromodulation and G protein–coupled receptor signaling. *Pharmacol. Rev.***6**, 1119–1139 (2023), 10.1124/pharmrev.122.000584.
26. W. Wei, A. V. Smrcka, Internalized beta2-Adrenergic receptors inhibit subcellular phospholipase C-dependent cardiac hypertrophic signaling. bioRxiv [Preprint] (2023). https://doi.org/10.1101/2023.06.07.544153 (Accessed 6 September 2023).
27. M. Stoeber *et al.*, A genetically encoded biosensor reveals location bias of opioid drug action. *Neuron* **98**, 963–976.e5 (2018).
28. A. Radoux-Mergault, L. Oberhauser, S. Aureli, F. L. Gervasio, M. Stoeber, Subcellular location defines GPCR signal transduction. *Sci. Adv.* **9**, eadf6059 (2023).
29. K. A. Ryall, J. J. Saucerman, Automated imaging reveals a concentration dependent delay in reversibility of cardiac myocyte hypertrophy. *J. Mol. Cell Cardiol.* **53**, 282–290 (2012).
30. M. Roth, A. Obaidat, B. Hagenbuch, OATPs, OATs and OCTs: The organic anion and cation transporters of the SLCO and SLC22A gene superfamilies. *Br. J. Pharmacol.* **165**, 1260–1287 (2012).
31. Y. Kato *et al.*, Involvement of influx and efflux transport systems in gastrointestinal absorption of celiprolol. *J. Pharm. Sci.* **98**, 2529–2539 (2009).
32. T. F. Solbach, M. Grube, M. F. Fromm, O. Zolk, Organic cation transporter 3: Expression in failing and nonfailing human heart and functional characterization. *J. Cardiovasc. Pharmacol.* **58**, 409–417 (2011).
33. T.-Y. Lin *et al.*, Cardiac contraction and relaxation are regulated by distinct subcellular cAMP pools. *Nat. Chem. Biol.* **1**, 62–73 (2024), 10.1038/s41589-023-01381-8.
34. A. M. Betiu *et al.*, Cell-permeable succinate rescues mitochondrial respiration in cellular models of amiodarone toxicity. *Int. J. Mol. Sci.* **22**, 11786 (2021).
35. A. J. Chruscinski *et al.*, Targeted disruption of the beta2 adrenergic receptor gene. *J. Biol. Chem.* **274**, 16694–16700 (1999).
36. D. G. Bailey, G. K. Dresser, B. F. Leake, R. B. Kim, Naringin is a major and selective clinical inhibitor of organic anion-transporting polypeptide 1A2 (OATP1A2) in grapefruit juice. *Clin. Pharmacol. Ther.* **81**, 495–502 (2007).
37. A. M. Schafer *et al.*, OATP1A2 and OATP2B1 are interacting with dopamine-receptor agonists and antagonists. *Mol. Pharm.* **17**, 1987–1995 (2020).
38. K. Lovgren, A. Hedberg, J. L. Nilsson, Adrenoceptor blocking agents. Compounds related to metoprolol. *J. Med. Chem.* **24**, 451–454 (1981).
39. L. C. Schneider, M. Mesa, E. Weisinger, P. Wiener, Solitary intramandibular neurofibroma: Report of a case. *J. Oral. Med.* **34**, 37–39 (1979).
40. X. Xu *et al.*, Binding pathway determines norepinephrine selectivity for the human beta(1)AR over beta(2)AR. *Cell Res.* **31**, 569–579 (2021).
41. M. V. Vargas *et al.*, Psychedelics promote neuroplasticity through the activation of intracellular 5-HT2A receptors. *Science* **379**, 700–706 (2023).

42. P. Poc *et al.*, Interrogating surface versus intracellular transmembrane receptor populations using cell-impermeable SNAP-tag substrates. *Chem. Sci.* **11**, 7871–7883 (2020).
43. M. Bathe-Peters *et al.*, Visualization of beta-adrenergic receptor dynamics and differential localization in cardiomyocytes. *Proc. Natl. Acad. Sci. U.S.A.* **118**, e2101119118 (2021).
44. G. Y. Mitronova *et al.*, High-affinity functional fluorescent ligands for human beta-adrenoceptors. *Sci. Rep.* **7**, 12319 (2017).
45. A. Duran-Corbera *et al.*, Caged-carvedilol as a new tool for visible-light photopharmacology of beta-adrenoceptors in native tissues. *iScience* **25**, 105128 (2022).
46. M. Gienger, H. Hubner, S. Lober, B. Konig, P. Gmeiner, Structure-based development of caged dopamine D(2)/D(3) receptor antagonists. *Sci. Rep.* **10**, 829 (2020).
47. S. R. Adams, R. Y. Tsien, Controlling cell chemistry with caged compounds. *Annu. Rev. Physiol.* **55**, 755–784 (1993).
48. M. Ricart-Ortega, J. Font, A. Llebaria, GPCR photopharmacology. *Mol. Cell Endocrinol.* **488**, 36–51 (2019).
49. A. Tadevosyan *et al.*, Caged ligands to study the role of intracellular GPCRs. *Methods* **92**, 72–77 (2016).
50. C. Merlen *et al.*, Intracrine endothelin signaling evokes IP3-dependent increases in nucleoplasmic Ca(2)(+) in adult cardiac myocytes. *J. Mol. Cell Cardiol.* **62**, 189–202 (2013).
51. Y. Wang *et al.*, Intracellular beta1-adrenergic receptors and organic cation transporter 3 mediate phospholamban phosphorylation to enhance cardiac contractility. *Circ. Res.* **128**, 246–261 (2021).
52. T. Morita *et al.*, pH-dependent transport kinetics of the human organic anion-transporting polypeptide 1A2. *Drug. Metab. Pharmacokinet.* **35**, 220–227 (2020).
53. J. Zheng *et al.*, PDZK1 and NHERF1 regulate the function of human organic anion transporting polypeptide 1A2 (OATP1A2) by modulating its subcellular trafficking and stability. *PLoS One* **9**, e94712 (2014).
54. J. H. Choi, J. W. Murray, A. W. Wolkoff, PDZK1 binding and serine phosphorylation regulate subcellular trafficking of organic anion transport protein 1a1. *Am. J. Physiol. Gastrointest. Liver Physiol.* **300**, G384–G393 (2011).
55. F. Zhou, A. C. Lee, K. Krafczyk, L. Zhu, M. Murray, Protein kinase C regulates the internalization and function of the human organic anion transporting polypeptide 1A2. *Br. J. Pharmacol.* **162**, 1380–1388 (2011).
56. M. Ackers-Johnson *et al.*, A simplified, langendorff-free method for concomitant isolation of viable cardiac myocytes and nonmyocytes from the adult mouse heart. *Circ. Res.* **119**, 909–920 (2016).
57. S. Bolte, F. P. Cordelieres, A guided tour into subcellular colocalization analysis in light microscopy. *J. Microsc.* **224**, 213–232 (2006).
58. D. Lang *et al.*, Calcium-dependent arrhythmogenic foci created by weakly coupled myocytes in the failing heart. *Circ. Res.* **121**, 1379–1391 (2017).
59. D. Lang *et al.*, Arrhythmogenic remodeling of beta2 versus beta1 adrenergic signaling in the human failing heart. *Circ. Arrhythm Electrophysiol.* **8**, 409–419 (2015).